EPIC 201702477b: A TRANSITING BROWN DWARF FROM K2 IN A 41 DAY ORBIT

Citation: Bayliss, D. et al. "EPIC 201702477b: A TRANSITING BROWN DWARF FROM K2 IN A 41 DAY ORBIT." The Astronomical Journal 153.1 (2016): 15. © 2016 The American Astronomical Society

As Published: http://dx.doi.org/10.3847/1538-3881/153/1/15

Publisher: IOP Publishing

Persistent URL: http://hdl.handle.net/1721.1/109493

Version: Final published version: final published article, as it appeared in a journal, conference proceedings, or other formally published context

The Astronomical Journal, 153:15 (10pp), 2017 January
doi:10.3847/1538-3881/153/1/15

EPIC 201702477b: A TRANSITING BROWN DWARF FROM *K2* IN A 41 DAY ORBIT

D. Bayliss[1,2], S. Hojjatpanah[3,4], A. Santerne[3,5], D. Dragomir[6,7,29], G. Zhou[8], A. Shporer[9,30], K. D. Colón[10,11], J. Almenara[12], D. J. Armstrong[13,14], D. Barrado[15], S. C. C. Barros[3], J. Bento[2], I. Boisse[5], F. Bouchy[1], D. J. A. Brown[13], T. Brown[16,17], A. Cameron[18], W. D. Cochran[19], O. Demangeon[5], M. Deleuil[5], R. F. Díaz[1], B. Fulton[20,31], K. Horne[18], G. Hébrard[21,22], J. Lillo-Box[23], C. Lovis[1], D. Mawet[24], H. Ngo[24], H. Osborn[13], E. Palle[25], E. Petigura[24,32], D. Pollacco[13], N. Santos[3,26], R. Sefako[27], R. Siverd[16], S. G. Sousa[3], and M. Tsantaki[3,28]

[1] Observatoire Astronomique de l'Université de Genève, 51 ch. des Maillettes, 1290 Versoix, Switzerland; daniel.bayliss@unige.ch
[2] Research School of Astronomy and Astrophysics, Australian National University, Canberra, ACT 2611, Australia
[3] Instituto de Astrofísica e Ciências do Espaço, Universidade do Porto, CAUP, Rua das Estrelas, 4150-762 Porto, Portugal
[4] Department of Physics, University of Zanjan, University Blvd., 45371-38791, Zanjan, Iran
[5] Aix Marseille Universite, CNRS, Laboratoire d'Astrophysique de Marseille UMR 7326, F-13388, Marseille, France
[6] The Department of Astronomy and Astrophysics, University of Chicago, 5640 S Ellis Ave., Chicago, IL 60637, USA
[7] Massachusetts Institute of Technology, Cambridge, MA 02139 USA
[8] Harvard-Smithsonian Center for Astrophysics, Cambridge, MA 02138, USA
[9] Jet Propulsion Laboratory, California Institute of Technology, 4800 Oak Grove Dr., Pasadena, CA 91109, USA
[10] NASA Ames Research Center, M/S 244-30, Moffett Field, CA 94035, USA
[11] Bay Area Environmental Research Institute, 625 2nd St. Ste 209 Petaluma, CA 94952, USA
[12] Univ. Grenoble Alpes, IPAG, F-38000 Grenoble, France
[13] Department of Physics, University of Warwick, Gibbet Hill Rd., Coventry, CV4 7AL, UK
[14] ARC, School of Mathematics and Physics, Queens University Belfast, University Rd., Belfast BT7 1NN, UK
[15] Depto. de Astrofísica, Centro de Astrobiología (CSIC-INTA), ESAC campus, E-28691 Villanueva de la Cañada, Spain
[16] Las Cumbres Observatory Global Telescope, Goleta, CA 93117, USA
[17] CASA, Department of Astrophysical and Planetary Sciences, University of Colorado, 389-UCB, Boulder, CO 80309, USA
[18] SUPA School of Physics and Astronomy, University of St. Andrews, KY16 9SS, UK
[19] McDonald Observatory and Department of Astronomy, Univeristy of Texas at Austin, TX, USA
[20] Institute for Astronomy, University of Hawaii, 2680 Woodlawn Dr., Honolulu, HI 96822-1839, USA
[21] Institut d'Astrophysique de Paris, UMR7095 CNRS, Université Pierre & Marie Curie, 98bis boulevard Arago, F-75014 Paris, France
[22] Observatoire de Haute-Provence, Universite d'Aix-Marseille & CNRS, F-04870 Saint Michel l'Observatoire, France
[23] European Southern Observatory (ESO), Alonso de Cordova 3107, Vitacura, Casilla 19001, Santiago de Chile, Chile
[24] California Institute of Technology, 1200 E. California Blvd., Pasadena, CA 91125, USA
[25] Instituto de Astrofísica de Canarias, E-38205 La Laguna, Tenerife, Spain
[26] Departamento de Física e Astronomia, Faculdade de Ciências, Universidade do Porto, Rua do Campo Alegre, 4169-007 Porto, Portugal
[27] South African Astronomical Observatory, P.O. Box 9, Observatory 7935, South Africa
[28] Instituto de Radioastronomía y Astrofísica, IRyA, UNAM, Campus Morelia, A.P. 3-72, C.P. 58089 Michoacán, Mexico

Received 2016 June 3; revised 2016 September 29; accepted 2016 October 14; published 2016 December 20

ABSTRACT

We report the discovery of EPIC 201702477b, a transiting brown dwarf in a long period (40.73691 ± 0.00037 day) and eccentric ($e = 0.2281 \pm 0.0026$) orbit. This system was initially reported as a planetary candidate based on two transit events seen in *K2* Campaign 1 photometry and later validated as an exoplanet candidate. We confirm the transit and refine the ephemeris with two subsequent ground-based detections of the transit using the Las Cumbres Observatory Global Telescope 1 m telescope network. We rule out any transit timing variations above the level of $\sim$30 s. Using high precision radial velocity measurements from HARPS and SOPHIE we identify the transiting companion as a brown dwarf with a mass, radius, and bulk density of $66.9 \pm 1.7\,M_{\rm J}$, $0.757 \pm 0.065\,R_{\rm J}$, and 191 ± 51 g cm^{-3} respectively. EPIC 201702477b is the smallest radius brown dwarf yet discovered, with a mass just below the H-burning limit. It has the highest density of any planet, substellar mass object, or main-sequence star discovered so far. We find evidence in the set of known transiting brown dwarfs for two populations of objects—high mass brown dwarfs and low mass brown dwarfs. The higher-mass population have radii in very close agreement to theoretical models, and show a lower-mass limit around $60\,M_{\rm J}$. This may be the signature of mass-dependent ejection of systems during the formation process.

Key words: planetary systems – techniques: photometric – techniques: spectroscopic

Supporting material: machine-readable table

1. INTRODUCTION

The scarcity of companions with masses between $13M_J$ and $80M_J$ around main sequence stars, the "brown dwarf desert," was first identified from numerous radial velocity planet searches (Halbwachs et al. 2000; Marcy & Butler 2000). Radial velocity surveys combined with astrometric data also show the brown dwarf desert to be real (Sahlmann et al. 2011; Wilson et al. 2016). Ground-based transit surveys, primarily sensitive to exoplanets with radii similar to or larger than Jupiter, seemed to confirm this desert by finding many Jupiter-mass objects, but very few brown dwarfs—see discoveries of WASP (Pollacco et al. 2006), HATNet (Bakos et al. 2004), HATSouth (Bakos et al. 2013), and KELT (Pepper et al. 2012).

---

[29] NASA Hubble Fellow.
[30] Sagan Fellow.
[31] NSF Graduate Research Fellow.
[32] Hubble Fellow.

In fact, of the 179 transiting planets discovered by these groups, only two, WASP-30b (Anderson et al. 2011) and KELT-1b (Siverd et al. 2012), have masses above 13 M_{J}. This is despite brown dwarfs having similar radii to hot Jupiters ($\sim 1\,R_{\mathrm{J}}$) and high mass objects being much easier to characterize with the routine radial velocity follow-up used by these projects. The space-based *CoRoT* mission (Rouan et al. 1999) discovered three transiting brown dwarfs: CoRoT-3b (Deleuil et al. 2008), CoRoT-15b (Bouchy et al. 2011b), and CoRoT-33b (Csizmadia et al. 2015). The *Kepler* mission uncovered another four transiting brown dwarfs: Kepler-39b (Bouchy et al. 2011a), KOI-205b (Díaz et al. 2013), KOI-415b (Moutou et al. 2013), and KOI-189b (Díaz et al. 2014b). Additionally KOI-554b and KOI-3728b have masses, measured via light curve modulations, just above 80 M_{J}, putting them very close to the brown dwarf regime (Lillo-Box et al. 2016). However the bulk of planet candidates discovered by the *Kepler* space mission (Borucki et al. 2010) have measured radii but not masses, so are not able to provide a constraint on the brown dwarf population due to the radius degeneracy between gas giants and brown dwarfs. The recent radial velocity study of Santerne et al. (2016) was able to measure the masses for a sample of large-radius *Kepler* candidates and found the occurrence rate of brown dwarfs with periods less than 400 days to be $0.29 \pm 0.17\%$. The extent of the brown dwarf desert was investigated in the study of Troup et al. (2016), which found that the brown dwarf desert only existed for orbital separations <0.1–0.2 au, and that beyond this brown dwarf companions appeared as numerous as low mass stellar companions. The study of Troup et al. (2016) probed a much wider range of spectral types and classes than typical RV or transit surveys, which may also be a factor in the high number of brown dwarf companions that they detected.

Brown dwarfs are thought to form via gravitational instability or molecular cloud fragmentation, whereas giant gas planets form via core accretion (Chabrier et al. 2014). However, it is possible that core accretion may produce super-massive planets in the 20–40 M_{J} range (Mordasini et al. 2009), and gravitational instability may also form gas giant planets (Nayakshin & Fletcher 2015). Thus the line between gas giants and brown dwarfs is a blurred one. It is argued that the distinction between these objects should be linked with formation mechanisms (Chabrier et al. 2014), and these different formation scenarios are almost certainly responsible for the brown dwarf desert rather than some observational bias (Ma & Ge 2014).

In this paper we report the discovery of a new transiting brown dwarf, EPIC 201702477b ($V = 14.57$), for which we can measure a precise mass and radius. In Section 2 we outline the photometric data from the *Kepler* space telescope and the Las Cumbres Observatory Global Telescope (LCOGT) 1 m network. We also describe the spectroscopic observations used to measure the radial velocities of EPIC 201702477 and to spectroscopically characterize the host star. We describe the high angular resolution imaging we carried out to further rule out blend scenarios. In Section 3 we carry out a joint analysis of the observational data in order to determine the physical and orbital characteristics of the transiting body. Finally, in Section 4 we look at the implications of this discovery in terms of the known population of well characterized brown dwarfs, the mass–radius–age relationship for brown dwarfs, and the evidence for a lower mass edge to the population of high mass brown dwarfs.

2. OBSERVATIONS

2.1. K2

The NASA *Kepler* telescope is a 0.95 m space-based Schmidt telescope with a 105 $\deg^2$ (Borucki et al. 2010) field of view (FOV). The original mission monitored a single field in the northern hemisphere, and was designed to determine the frequency of Earth-like planets in the galaxy. After four years of operations two of the spacecraft's reaction wheels failed, ending the original mission. However, the telescope was re-purposed to monitor selected ecliptic fields, which optimizes the pointing stability, in a new mission called *K2* (Howell et al. 2014).

K2 monitors pre-selected target stars in ecliptic fields for durations of approximately 80 days. While this duration is much shorter than the original *Kepler* mission, it is still a significant improvement over ground-based monitoring which must contend with interruptions from poor weather and the Earth's day–night cycle. The result of this is that *K2* is currently the premier facility for finding long period transiting planets, and EPIC 201702477b is an example of such a discovery.

EPIC 201702477 was monitored by *K2* as part of Campaign 1 between 2014 May 30 and August 21. The star was included as part of program GO1059 (Galactic Archaeology), which aimed to monitor red giant stars and selected targets based purely on a 2MASS magnitude and color cut. The 2MASS color of EPIC 201702477 is $J - K = 0.502$, right at the edge of the color cut for the program ($J - \mathrm{K} > 0.5$). Given this and the magnitude of the target ($V = 14.57$), it was not likely EPIC 201702477 would be a giant star, and indeed our spectroscopy shows the star is a Sun-like dwarf (see Section 2.3).

EPIC 201702477b was first identified as a transiting exoplanet candidate in Foreman-Mackey et al. (2015), where a transit signal with a 40.7365 day periodicity was reported. The candidate was studied further by Montet et al. (2015b) using existing Sloan Digital Sky Survey (SDSS) imaging, and they noted the presence of a neighbor at $12\overset{\prime\prime}{.}11$ with a $\Delta r = 4.65 \pm 0.09$ mag. They concluded this neighbor was not sufficiently close to be responsible for the transit signal identified using a photometric aperture with a size of $10''$. They also calculated the false positive probability (FPP) for EPIC 201702477b using the VESPA algorithm (Morton 2012) to be 0.145, and therefore deemed it to be an "exoplanet candidate" (defined as $0.01 < \mathrm{FFP} < 0.9$).

Due to its long orbital period there are only two transit events in the *K2* data, and at the *K2* 30 minute cadence this equated to just 16 in-transit data points. Such poor sampling of the transit event, even given the exquisite precision of *K2*, meant that the transit parameters were rather poorly defined. In such circumstances, further ground-based photometry is very important in order to help fully characterize the system.

Of the 37 candidates presented by Foreman-Mackey et al. (2015), EPIC 201702477 has the longest orbital period, with the exception of EPIC 201257461, which has been shown to be a false candidate (Montet et al. 2015b). The reported planet/star radius ratio of EPIC 201702477b is $R_P/R_{\mathrm{star}} = 0.0808$, indicating a gas giant exoplanet assuming a solar-type host.

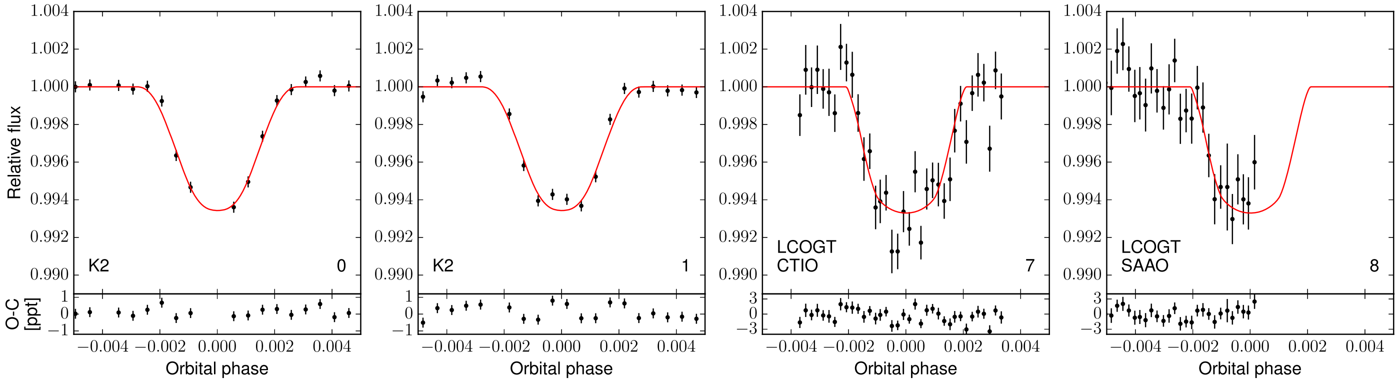

Figure 1. Transit light curves for EPIC 201702477 phase-folded to the best fitting period of $P = 40.73691 \pm 0.00037$ day. Black circles are the photometric data points, while the red line is the best-fit transit model. The first two light curves are the *K2* data, comprising two transit events in the *Kepler* bandpass. The third light curve is the LCOGT 1 m+Sinistro *r*-band light curve from a single transit event observed from CTIO, Chile on 2015 March 15. The fourth light curve is the LCOGT 1 m+SBIG *r*-band light curve from a single transit event observed from SAAO, South Africa on 2015 April 28.

We downloaded the *K2* pixel data for EPIC 201702477 from the Mikulski Archive for Space Telescopes (MAST)[33] and used a modified version of the *CoRoT* imagette pipeline (Barros et al. 2015) to extract the light curve. We computed an optimal aperture based on signal-to-noise of each pixel. The background was estimated using the 3σ clipped median of all the pixels in the image outside the optimal aperture and removed before aperture photometry was performed. We also calculated the centroid using the modified moment method by Stone (1989). For EPIC 201702477 we found that a 14 pixel photometric aperture resulted in the best photometric precision.

The degraded pointing stability of the *K2* mission results in flux variations correlated with the star's position on the CCD. To correct for this we used a self-flat-fielding procedure similar to Vanderburg & Johnson (2014) that assumes the movement of the satellite is mainly in one direction. A full description of the pipeline given in Barros et al. (2016). The final light curve of EPIC 201702477 has mean out-of-transit rms of 293 ppm and the two transit events in the light curve are plotted in Figure 1.

2.2. LCOGT

The LCOGT is a network of fully automated telescopes (Brown et al. 2013). Currently there are 10 LCOGT 1 m telescopes operating as part of this network, eight of which are in the southern hemisphere: three at the Cerro Tololo Inter-American Observatory (CTIO) in Chile, three at the South African Astronomical Observatory (SAAO) in South Africa, and two at Siding Spring Observatory (SSO) in Australia. Each telescope is equipped with an imaging camera; either a “Sinistro” or an SBIG STX-16803. The Sinistro is LCOGT's custom built imaging camera that features a back-illuminated 4 K × 4 K Fairchild Imaging CCD with 15 μm pixels (CCD486 BI). With a plate scale of $0\farcs387$/pixel, the Sinistro cameras deliver a FOV of $26\farcm6 \times 26\farcm6$, which is important for monitoring a sufficient number of reference stars for high-precision differential photometry. The cameras are read out by four amplifiers with 1 × 1 binning, with a readout time of ≈45 s. The SBIG STX-16803 cameras are commercial CCD cameras which feature a frontside-illuminated 4 K × 4 K CCD with 9 μm pixels—giving a field of view of $15\farcm8 \times 15\farcm8$. These cameras are typically read out in 2 × 2 binning mode, which results in a read-out time of 12 s.

The Transiting Exoplanet CHaracterisation (TECH)[34] project uses the 1 m telescopes in the LCOGT network to photometrically characterize transiting planets and transiting planet candidates. A major focus of the TECH project is to characterize long period (>10 day) transiting planets or candidates which are difficult to monitor with single site or non-automated telescope systems. As such, EPIC 201702477 was selected as a good candidate for photometric monitoring, and was entered into the automated observing schedule in 2015 February.

The first transit event for EPIC 201702477b monitored by the TECH project was on 2015 March 15 from CTIO. We observed the target from 01:00 UT to 08:13 UT using a Sinistro in the *r*-band. The exposure times were 240 s, the observing conditions were photometric, and the airmass ranged from 2.3 to 1.2. We detected a full transit of EPIC 201702477b with a depth and duration consistent with that seen in the *K2* data. The next transit event occurred 41 days later on 2015 April 28, and was observable from SAAO. EPIC 201702477 was monitored between 17:00 UT and 22:50 UT using an SBIG camera, again in the *r*-band. The exposure times were 180 s, the observing conditions were again photometric, and the airmass ranged from 1.8 to 1.2. These data show the first half of a transit event consistent with the previous events. The images for both observations were calibrated via the LCOGT pipeline (Brown et al. 2013) and aperture-photometry extracted in the standard manner as set out in Penev et al. (2013). The photometric data are provided in Table 1, and the phase-folded light curves are presented in Figure 1.

2.3. Spectral Typing

In order to determine the stellar parameters for EPIC 201702477, on 2015 March 2 we obtained a low-resolution (R = 3000) spectrophotometric observation with the Wide Field Spectrograph (WiFeS) on the Australian National University (ANU) 2.3 m telescope at SSO. The methodology for this spectral typing is fully set out in Bayliss et al. (2013). A spectrum of $R = \lambda/\Delta\lambda = 3000$ from 3500 to 6000 Å is flux calibrated according to Bessell (1999) using spectrophotometric standard stars. We determine stellar properties,

---

[33] archive.stsci.edu/k2/

[34] lcogt.net/science/exoplanets/tech-project/

Table 1
r-band Differential Photometry for EPIC 201702477 from LCOGT 1 m

BJD (2,400,000+)	Rel. Flux	Rel. Flux Error	Site/Instrument
57096.5492063002	1.0000	0.0018	CTIO/Sinistro
57096.5525186099	1.0047	0.0018	CTIO/Sinistro
57096.5558380098	1.0008	0.0018	CTIO/Sinistro
57096.5591604202	1.0025	0.0018	CTIO/Sinistro
57096.5624648202	1.0038	0.0017	CTIO/Sinistro
57096.5657806299	1.0019	0.0017	CTIO/Sinistro
57096.5690742298	1.0030	0.0017	CTIO/Sinistro
57096.5723725399	1.0023	0.0017	CTIO/Sinistro
57096.5756765502	1.0015	0.0017	CTIO/Sinistro

(This table is available in its entirety in machine-readable form.)

particularly $T_{\rm eff}$ and $\log g$, via a grid search using the synthetic templates from the MARCS model atmospheres (Gustafsson et al. 2008). The results showed the star was a Sun-like dwarf star with $T_{\rm eff} = 5600 \pm 200$ K and $\log g = 4.5 \pm 0.5$ dex. Thus the transit depth was confirmed to be consistent with a planetary-size body.

To better determine the stellar properties we obtained a spectrum of the star with Keck/HiReS (Vogt et al. 1994) on 2015 June 30. The instrument was configured to the standard setup for the California Planet Search (Howard et al. 2010). We collected a single 7 minutes exposure using the C2 (14 × 0.861) decker for a spectral resolution of $R \sim 45{,}000$ and signal-to-noise ratio (S/N) of ~25 per pixel at 5500 Å. We used the software SPECMATCH (Petigura 2015) to determine the stellar properties. The resulting parameters are listed as initial spectroscopic information in Table 2. Following the methodology described in Sozzetti et al. (2007) we used these initial spectral parameters from Keck as priors for the global fitting (see Section 3), determined a new $\log g$, and then used this as a prior for a second iteration of SPECMATCH. The global fit was then run again with these updated parameters, and the final solution gave $T_{\rm eff} = 5517 \pm 70$ K and $\log g = 4.466 \pm 0.058$ for EPIC 201702477. The final set of stellar parameters is listed in Table 4.

2.4. Lucky and AO Imaging

We obtained a high-spatial resolution image with the instrument AstraLux (Hormuth et al. 2008), mounted on the 2.2 m telescope in Calar Alto Observatory (Almería, Spain), using the lucky imaging technique. The target was observed on 2015 November 18 under normal weather conditions. We obtained 60,000 frames with individual exposure times of 0.060 s, hence a total exposure time of 1 hour, in the SDSS *i*-band. The images were reduced using the observatory pipeline, which applies bias and flat-field correction to the individual frames and selects the best images in terms of Strehl ratio (Strehl 1902). The best 10% of the images are then aligned and stacked to compose the final image. The sensitivity limits are calculated following the process explained in Lillo-Box et al. (2014) and are presented in Figure 2.

We observed EPIC 201702477 on 2015 December 27 using NIRC2 NGS-AO (PI: Keith Matthews) on Keck II. We used the *Ks* band and the narrow camera setting. We took a total of four images, each with 60 s of total integration time. We calibrated the images with a flat field, dark frames, and removed image artifacts from dead and hot pixels. We then created a single median-stacked image. We do not see any stellar companions in this image, and compute the contrast curve from the median stacked image. For every point in the image, we compute the total flux from pixels within a box with side length equal to the full width at half maximum (FWHM) of the target star's point-spread function (PSF). We then divide the image into a series of annuli with width equal to twice the

Table 2
Summary of Stellar Properties for EPIC 201702477

Parameter	Value	Source
Identification		
R.A. (deg.)	175.2407940	*K2* EPIC
Decl. (deg.)	+3.6815840	*K2* EPIC
2MASS ID.	11405777 + 0340535	2MASS PSC
Photometric Information		
Kepler (mag)	14.430	*K2* EPIC
u (mag)	16.312 ± 0.005	SDSS DR12
g (mag)	14.871 ± 0.003	SDSS DR12
r (mag)	14.354 ± 0.003	SDSS DR12
i (mag)	14.189 ± 0.003	SDSS DR12
z (mag)	14.137 ± 0.004	SDSS DR12
J (mag)	13.268 ± 0.027	2MASS PSC
H (mag)	12.881 ± 0.028	2MASS PSC
K (mag)	12.766 ± 0.033	2MASS PSC
Space Motion		
pmR.A. (mas $\rm yr^{-1}$)	−10.0 ± 3.6	PPMXL
pmDec (mas $\rm yr^{-1}$)	−9.8 ± 3.6	PPMXL
mean $\gamma_{\rm RV}$ (km $\rm s^{-1}$)	34.0	HARPS
Initial Spectroscopic Information		
$T_{\rm eff}$ (K)	5492 ± 60	Keck
$\log g$	4.12 ± 0.07	Keck
[Fe/H]	−0.20 ± 0.04	Keck
$v \sin i$(km $\rm s^{-1}$)	<2	Keck

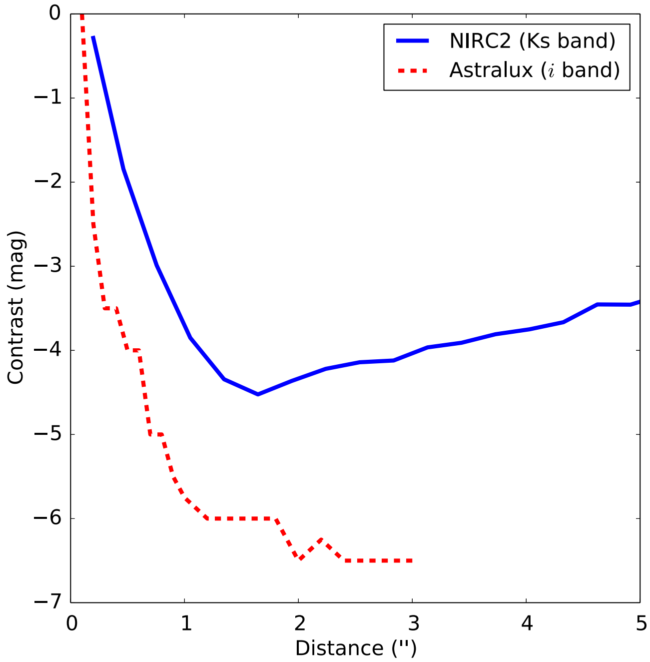

Figure 2. 5-sigma contrast curves for EPIC 201702477 from imaging observations. Blue solid line: Keck/NIRC2 K-band imaging. Red dashed line: Astralux lucky imaging.

Table 3
SOPHIE and HARPS RVs of EPIC 201702477

BJD (2,400,000+)	RV (km s^{-1})	σ_{RV} (km s^{-1})	V_{span} (km s^{-1})	$\sigma_{V_{\mathrm{span}}}$ (km s^{-1})	FWHM (km s^{-1})	σ_{FWHM} (km s^{-1})	Texp (s)	S/N	Instrument
57363.71073	37.566	0.025	−0.066	0.045	9.595	0.062	3600	21.7	SOPHIE
57399.62998	35.780	0.046	0.103	0.082	9.614	0.114	3600	13.7	SOPHIE
57436.62181	33.236	0.031	0.129	0.055	9.251	0.076	1800	8.2	SOPHIE
57397.85193	34.765	0.011	−0.031	0.016	6.744	0.022	3600	12.0	HARPS
57401.81118	36.943	0.007	0.002	0.010	6.709	0.013	3600	17.5	HARPS
57404.83131	37.670	0.050	0.033	0.075	7.004	0.100	900	3.0	HARPS
57407.80298	38.103	0.041	−0.117	0.061	6.802	0.082	1500	5.5	HARPS
57410.77375	37.918	0.056	−0.091	0.084	6.311	0.111	900	2.9	HARPS
57417.80853	36.254	0.041	0.108	0.061	6.574	0.081	900	3.9	HARPS
57424.79651	32.335	0.039	−0.080	0.058	6.912	0.078	900	4.2	HARPS
57427.78748	30.393	0.033	0.000	0.050	6.827	0.067	900	4.8	HARPS
57429.80114	29.672	0.053	0.079	0.079	6.797	0.106	900	3.1	HARPS
57433.79557	30.881	0.045	0.005	0.067	6.803	0.090	900	3.8	HARPS

Note. S/N is given per pixel at 550 nm.

FWHM. For each annulus, we determine the 1σ contrast limit to be the standard deviation of the total flux values for boxes inside that annulus. To convert from flux limits to flux ratios and differential magnitudes, we divide the computed standard deviation by the total flux of a similar box centered on the target star. Figure 2 shows the 5σ average contrast curve.

The clear conclusion from both the lucky imaging and the AO imaging is that the target appears to be an isolated star to within the limits presented in our contrast curves, and this indicates the transit is occurring on the target star rather than a nearby blended neighbor.

2.5. Radial Velocities

We performed radial velocity follow-up observations of EPIC 201702477 with the SOPHIE (Bouchy et al. 2009a) and HARPS (Mayor et al. 2003) spectrographs. Both instruments are high-resolution ($R \approx 40{,}000$ and 110,000 for SOPHIE and HARPS, respectively), fiber-fed, and environmentally controlled echelle spectrographs covering visible wavelengths. We obtained three spectra with SOPHIE (OHP programme ID: 15B.PNP.HEBR) from 2015 June 12 to 2016 February 17 with exposure times of 1800 and 3600 s, reaching an S/N between 8 and 22 per pixel at 5500 Å. We obtained 10 other spectra with HARPS (ESO programme ID: 096.C-0657) from 2016 January 10 to February 15 with exposure times between 900 and 3600 s, corresponding to an S/N between 3 and 17 per pixel at 5500 Å.

All spectra were reduced with the online pipeline available at the telescopes. The spectra were then cross-correlated with a template mask that corresponds to a G2V star (Baranne et al. 1996). This template was chosen to be close in spectral type to the host star. Radial velocities, bisector span, and FWHM were measured on the cross-correlation function and their associated uncertainties were estimated following the methods described in Bouchy et al. (2001), Boisse et al. (2010), and Santerne et al. (2015). SOPHIE radial velocities were corrected for charge-transfer inefficiency (Bouchy et al. 2009b) using the equation provided in Santerne et al. (2012). The derived radial velocities are reported in Table 3 and plotted in Figure 3.

Our radial velocity measurements show a large amplitude ($K = 4.252 \pm 0.028\ \mathrm{km\ s^{-1}}$) variation in-phase with the photometric ephemeris and indicative of a brown dwarf mass companion in an elliptical orbit. We use these radial velocity data to determine the planetary parameters in Section 3.

3. ANALYSIS

3.1. Joint Analysis

We analyzed the radial velocity and photometric data of EPIC 201702477 with the Markov chain Monte Carlo (MCMC) algorithm of the PASTIS software, which is fully described in Díaz et al. (2014a). We modeled the radial velocities with a Keplerian orbit and the photometric data with the JKTEBOP package (Southworth 2011) and references therein. We chose as a prior for the stellar parameters the values derived from the Keck spectroscopy (Section 2.3). We used the Dartmouth stellar evolution tracks of Dotter et al. (2008) to derive the stellar fundamental parameters (mass, radius, age) in the MCMC, in particular the stellar density which was used to constrain the transit parameters given the eccentricity constrained by the radial velocities, as in Santerne et al. (2014). We ignored pre-main sequence solutions as there is no evidence that this is a young star and the pre-main sequence stage is extremely short in duration. We assumed uninformative priors for the parameters, except for the orbital ephemeris for which we used the ones provided by Montet et al. (2015b), the spectroscopic parameters that we took from our spectral analysis, and the orbital eccentricity for which we choose a Beta distribution as recommended by Kipping (2013). For the transit modeling, we used a quadratic law with coefficients taken from the interpolated table of Claret & Bloemen (2011) for both the *Kepler* and *r* bandpasses and changed them at each step of the MCMC.

We ran 20 chains of 3×10^5 iterations each, with starting points randomly drawn from the joint prior. We rejected non-converged chains based on the Kolmogorov–Smirnov test (Díaz et al. 2014a). We then removed the burn-in of each chain before thinning and merging them. We ended with more than 3000 independent samples of the posterior distribution that we used to derive the value and 68.3% uncertainty of each parameter that we report in Table 4.

We also modeled the system independently (but with the same datasets) using the EXOFAST software (Eastman et al. 2013). We find parameters and uncertainties in close

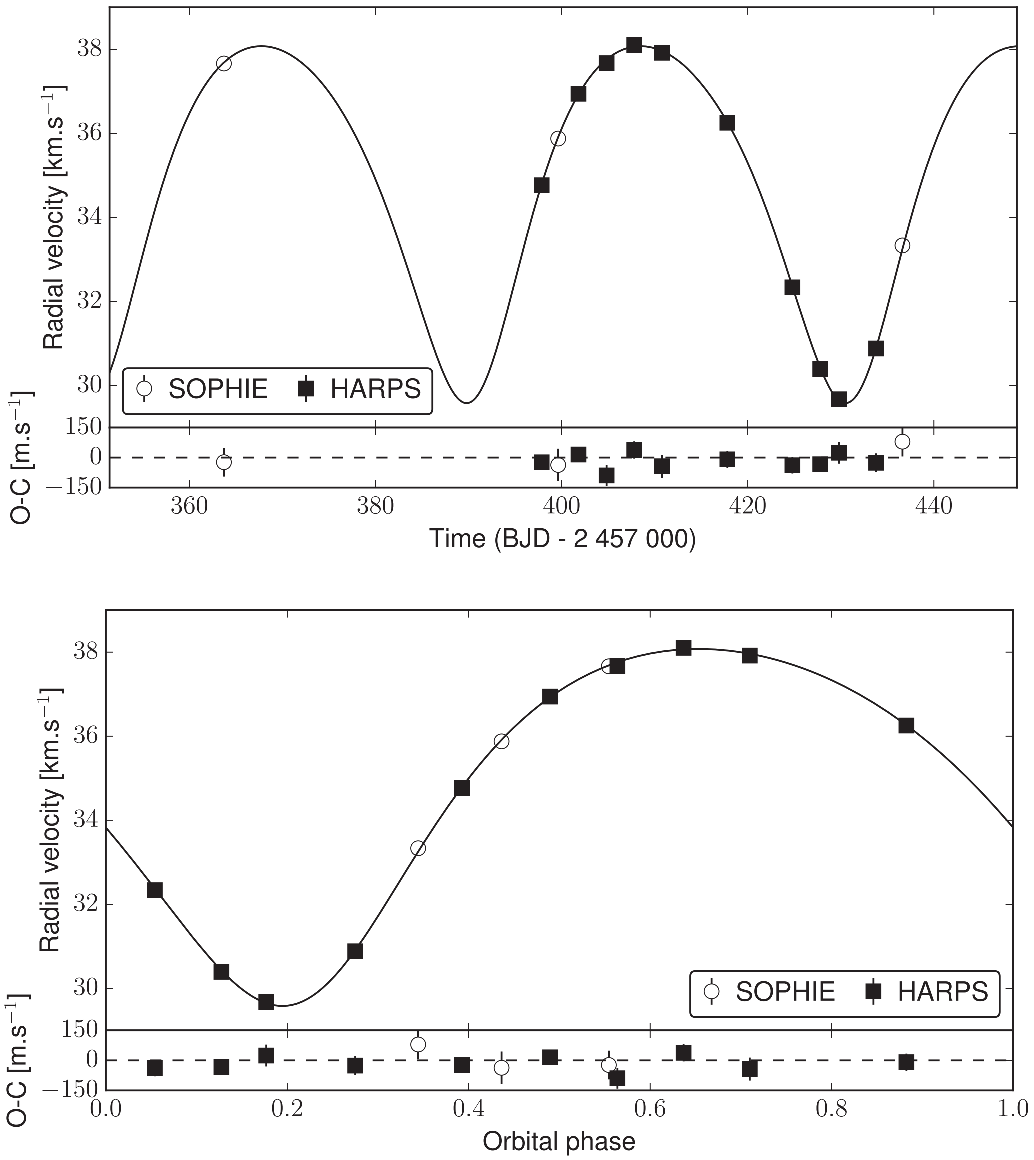

Figure 3. Top: radial velocity measurements for EPIC 201702477 from the HARPS (solid squares) and SOPHIE (empty circles) spectrographs plotted against time. The black line shows the best fit global model (see Section 3.1). The lower inset panel shows *O–C* residuals from this best fit model. Bottom: same as above, but phase-folded to the best-fit period of $P = 40.73691 \pm 0.00037$ day.

agreement with those that were derived using PASTIS, and therefore we only report the PASTIS results.

3.2. TTV Analysis

In order to test for transit timing variations (TTVs), we perform an independent fit of the *K*2 and LCOGT transit light curves. We fit for independent centroids T_0 for each transit, while forcing the transits to share the geometric parameters $a/R_\star$, $R_{\rm BD}/R_\star$, and i. Since ground-based photometry suffers from instrumental systematics that can bias the centroid measurements, we simultaneously detrend the LCOGT light curves against a linear combination of the terms describing the time, X, Y pixel drift, airmass trend, sky background flux, and target star FWHM variations. No significant TTVs were detected at the 30 s level. The high cadence LCOGT light curves offer similar timing precisions as the long cadence *K*2 observations, and demonstrate the power of follow-up observations for long period candidates from *K*2. The variations in the transit centroid times are shown in Figure 4 and listed in Table 5.

3.3. Out-of-transit Light Curve Analysis

We can place an upper limit on the companion's luminosity based on the secondary eclipse measurements. We checked for the presence of a secondary eclipse in the *K2* light curves; the phase of the eclipse is constrained by a Gaussian prior on the e and ω orbital parameters, determined from the RV observations and presented in Table 4. No secondary eclipse is detected at a 2σ upper limit of 1.96 mmag, equating to a maximum blackbody temperature for the brown dwarf of $T_{\rm eff} < 3950$ K.

4. DISCUSSION

With a period just over 40 days, EPIC 201702477b is the second longest period transiting brown dwarf discovered to date. The discovery of long-period transiting systems from the *K2* data is encouraging, as such systems are extremely difficult

Table 4
Parameters from the Global Fit for the EPIC 201702477 System

Parameter	Value
Brown Dwarf	
P (days)	40.73691 ± 0.00037
T_0 (BJD)	2456811.5462 ± 0.0011
T_{14} (hr)	4.04 ± 0.13
$a/R_\star$	54.0 ± 3.4
$R_{\mathrm{BD}}/R_\star$	0.0862 ± 0.0024
b	0.851 ± 0.023
b_{sec}	0.752 ± 0.023
i (degrees)	89.105 ± 0.082
e	0.2281 ± 0.0026
ω (degrees)	195.9 ± 1.8
γ_{RV} (km s^{-1})	34.745 ± 0.020
K (km s^{-1})	4.252 ± 0.028
$M_{\mathrm{BD}}(M_{\mathrm{J}})$	66.9 ± 1.7
$R_{\mathrm{BD}}(R_{\mathrm{J}})$	0.757 ± 0.065
a (au)	0.2265 ± 0.0026
ρ_c (g cm^{-3})	191 ± 51
Star	
$\log g$	4.466 ± 0.058
T_{eff} (K)	5517 ± 70
[Fe/H]	−0.164 ± 0.053
$R_\star$ ($R_\odot$)	0.901 ± 0.057
$M_\star$ ($M_\odot$)	0.870 ± 0.031
$\rho_\star$ ($\rho_\odot$)	1.18 ± 0.24
age (Gyr)	8.8 ± 4.1
RV and Photometry	
HARPS jitter (km s^{-1})	$0.035^{+0.031}_{-0.018}$
SOPHIE jitter (km s^{-1})	$0.101^{+0.180}_{-0.070}$
SOPHIE offset relative to HARPS (km s^{-1})	0.078 ± 0.081
K2 contamination	$0.0071^{+0.0072}_{-0.0049}$
K2 flux out of transit	1.000022 ± 3.4e-05
K2 jitter	0.000253 ± 2.8e-05
SAAO contamination	$0.030^{+0.030}_{-0.021}$
SAAO flux out of transit	0.99975 ± 2.7e-04
SAAO jitter	0.00039 ± 3.8e-04
CTIO contamination	$0.025^{+0.028}_{-0.018}$
CTIO flux out of transit	0.99966 ± 2.0e-04
CTIO jitter	0.00089 ± 3.2e-04

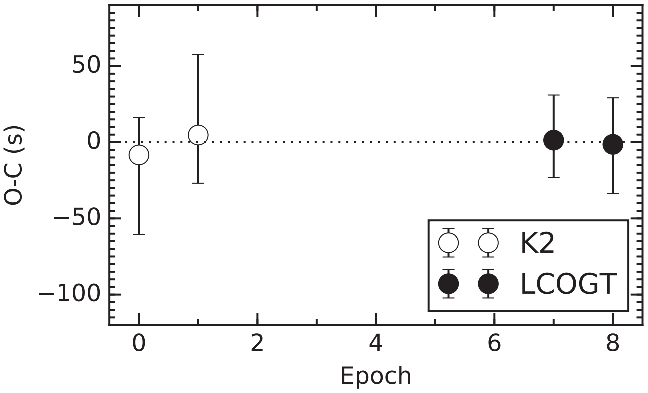

Figure 4. Transit timing variations for EPIC 201702477b for four transits (epochs 0 and 1 from *K2* data, epochs 7 and 8 from LCOGT data). The dotted line indicates the mean $O-C$ offset. We do not observe any variation at the level of ∼30 s.

Table 5
Summary of Photometric Observations for EPIC 201702477

Instrument	Epoch	Transit Centroid (BJD-TDB)	Filter
Kepler	0	$2456811.54499(^{+28}_{-60})$	Kep.
Kepler	1	$2456852.28205(^{+61}_{-37})$	Kep.
LCOGT 1 m+Sinistro	7	$2457096.70347(^{+34}_{-28})$	sloan-r
LCOGT 1 m+SBIG	8	$2457137.44035(^{+35}_{-38})$	sloan-r

to find from ground-based surveys; HATS-17b (Brahm et al. 2016) being the current record at 16.3 days. Long-period systems will remain difficult to discover even when the *Transiting Exoplanet Survey Satellite* (*TESS*) mission is operating (Ricker et al. 2014) as most fields in this survey will only be monitored for 27 days. EPIC 201702477b also demonstrates that like the *Kepler* mission, some fraction of the *K2* validated planets may turn out not to be planets, even at radii down to 0.75 R_{J}, due to confusion with brown dwarf companions.

4.1. Populating The Brown Dwarf Desert

Including EPIC 201702477b, there are just 12 known brown dwarfs ($13M_{\mathrm{J}} < M_{\mathrm{BD}} < 80M_{\mathrm{J}}$) that transit main sequence stars —see Table 6 for a list and Csizmadia et al. (2015) for a detailed list of these systems. These systems are extremely important as they provide an independent check on the radial velocity statistics for brown dwarfs, in addition to giving us true masses and radii. While a full statistical analysis is beyond the scope of this paper, we note that from the *K2* survey alone there have been five previously unknown hot Jupiter discoveries (NASA Exoplanet Archive on 2016 April 20), but EPIC 201702477b is the first brown dwarf discovery. Although this is in line with the relative statistics for these two populations presented in Santerne et al. (2016), we caution that the target selection process for *K2* imprints a strong bias on the sample and makes robust statistics dependent on careful modeling of the selection effects. In addition, the detection of a large radial velocity variation may prompt follow-up efforts to be discontinued for some planet search programs.

4.2. Two Populations of Brown Dwarfs

Ma & Ge (2014) have suggested that there exist two populations of brown dwarfs. The first are brown dwarfs below ∼45 M_{J} that are formed in the protoplanetary disc via gravitational instability. The second are brown dwarfs above ∼45 M_{J} that are formed through molecular cloud fragmentation; essentially the very lowest mass objects of the star formation process. This division of the brown dwarf population at ∼45 M_{J} coincides with the minimum of the companion mass function derived by Grether & Lineweaver (2006) and the void in the mass range as derived from the CORALIE RV survey (Sahlmann et al. 2011). Under this division, EPIC 201702477b would clearly be classed in the second category as likely to be formed via molecular cloud fragmentation, as at 66.9 ± 1.7 M_{J} its mass lies well above the mass division.

Unlike pure RV detections, transiting brown dwarfs can have true masses determined, as opposed to minimum masses. We can also be fairly certain that these discoveries are free from a mass bias, as to first order the discoveries are made on the basis of the planet-to-star radius ratio alone, and radius of the companion is largely independent of the mass in the brown dwarf regime. Therefore while the numbers are still small, transiting brown dwarfs provide a critical test of the two-population model proposed in Ma & Ge (2014). As can be seen

Table 6
Brown Dwarfs Transiting Main Sequence Stars

Name	Period (days)	Mass (M_J)	Radius (R_J)	Metallicity [Fe/H]	Age (Gyr)	Reference
CoRoT-3b	4.256	21.23 ± 0.82	0.993 ± 0.058	−0.02 ± 0.06	2.2	Deleuil et al. (2008), Triaud et al. (2009)
NLTT41135b	2.889	33.7 ± 2.8	1.13 ± 0.27	−0.25 ± 0.25	5.0	Irwin et al. (2010)
CoRoT-15b	3.060	63.3 ± 4.1	1.12 ± 0.30	+0.1 ± 0.2	2.24	Bouchy et al. (2011b)
WASP-30b	4.156	60.96 ± 0.89	0.889 ± 0.021	−0.08 ± 0.10	1.5	Anderson et al. (2011)
LHS6343C	12.713	62.1 ± 1.2	0.783 ± 0.011	+0.02 ± 0.19	5.0	Johnson et al. (2011), Montet et al. (2015a)
Kepler-39b (KOI-423b)	21.087	19.1 ± 1.0	1.11 ± 0.03	+0.10 ± 0.14	1.0	Bouchy et al. (2011a), Bonomo et al. (2015)
KELT-1b	1.217	27.38 ± 0.93	1.116 ± 0.038	+0.052 ± 0.079	1.75	Siverd et al. (2012)
KOI-205b	11.720	40.8 ± 1.5	0.82 ± 0.02	+0.18 ± 0.12	1.7	Díaz et al. (2013), Bonomo et al. (2015)
KOI-415b	166.788	62.14 ± 2.69	0.79 ± 0.12	−0.24 ± 0.11	10.5	Moutou et al. (2013)
KOI-189b	30.360	78.0 ± 3.4	0.998 ± 0.023	−0.07 ± 0.12	6.1	Díaz et al. (2014b)
CoRoT-33b	5.819	59.0 ± 1.8	1.10 ± 0.53	+0.44 ± 0.10	7.8	Csizmadia et al. (2015)
EPIC 201702477b	40.737	66.9 ± 1.7	0.757 ± 0.065	−0.16 ± 0.05	8.8	this work

from Figure 5, we do indeed see evidence of a gap in the mass distribution between about 40 and 55 M_J, lending support to the two-population hypothesis.

We also investigate if these populations of brown dwarfs correlate with the metallicity of the host stars they transit. In line with the well established relationship of giant planet frequency increasing with host metallicity (Gonzalez 1997; Santos et al. 2001; Fischer & Valenti 2005), we may expect the lower mass brown dwarfs, if formed by core-accretion, to orbit higher metallicity host stars than the higher mass brown dwarfs that formed by fragmentation. With the current sample of just 12 transiting brown dwarfs we do not observe any such correlation; see Figure 6.

4.3. Mass–Radius–Age Relationship for Brown Dwarfs

EPIC 201702477b lies at the minimum for brown dwarf radii, and with a density of 191 ± 51 g cm^{-3} it is the highest density object ever discovered in the regime from planets to main sequence stars—see Figure 7. To investigate the mass–radius relationship for brown dwarfs we take the known systems with precise (uncertainties <20%) mass and radius and compare the measured radius with the radius predicted from the COND03 models (Baraffe et al. 2003). We use the published masses and ages for each transiting brown dwarf (set out in Table 6), and compute a COND03 model radius for each object based on a two-dimensional (2D) linear interpolation of the model grid points. We plot the difference between the measured radius and these computed radii in Figure 8. For hot Jupiters, there exists a population of inflated radius objects at short periods where the insolation flux exceeds 10^8 erg cm^{-2} s^{-1} (Demory & Seager 2011). However for brown dwarfs the radii do not appear to exhibit such a trend, and the radii appear to be uncorrelated with the insolation flux (or for that matter orbital period). This may be expected as most of the mechanisms proposed for giant planet inflation do not apply to these more massive brown dwarfs (Bouchy et al. 2011b). A possible exception may be KELT-1b (Siverd et al. 2012) which receives extremely high insolation of 7.81×10^9 erg cm^{-2} s^{-1} and indeed appears to be inflated. However we do note that the higher mass population of brown dwarfs are in much closer agreement to the COND03 models than the lower mass population of brown dwarfs (see Figure 8).

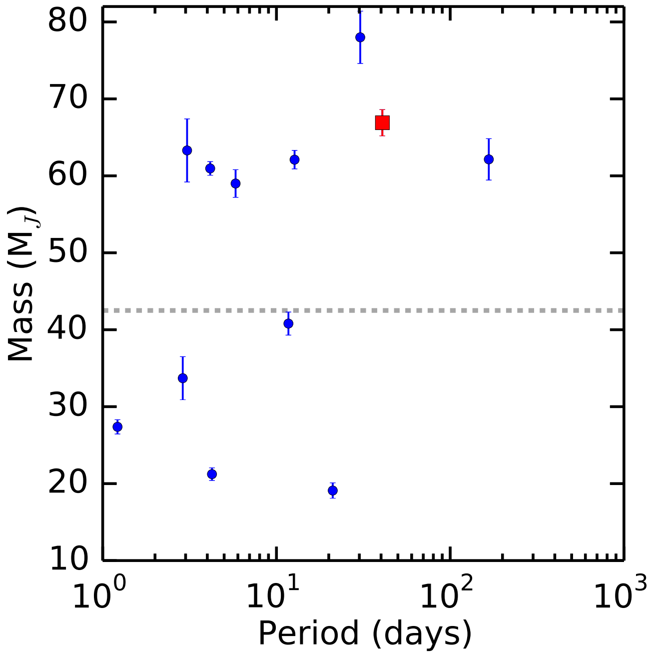

Figure 5. Masses of all known brown dwarfs that transit main sequence host stars plotted against their orbital periods. Blue circles are from the literature (see Table 6), while the red square is EPIC 201702477b. We note that EPIC 201702477b has the second longest period of all these discoveries. The dashed gray line indicates the 42.5M_J mass at which Ma & Ge (2014) report a gap in the mass distribution. Based on these transiting systems alone, we do indeed see evidence for such a gap with roughly equal numbers of companions discovered in each population.

4.4. The Mass Edge at 60 M_J

Of the 12 known transiting brown dwarfs, six have masses in the range of 59–67 M_J, as shown in Figure 5. The lack of higher mass objects is only because we restricted our sample to objects less than 80 M_J(the usual limit for what is considered a brown dwarf). Many transit and radial velocity surveys may also not report objects above this mass. However the lack of discoveries with masses below this group of high mass transiting brown dwarfs is interesting, and appears as a sharp lower mass edge to the high-mass brown dwarfs. While we caution that the sample size is still small, the edge is intriguing and may be related to the ejection process during formation. In the simulations of Stamatellos & Whitworth (2009) it was found that although the formation of brown dwarfs is approximately flat in the regime

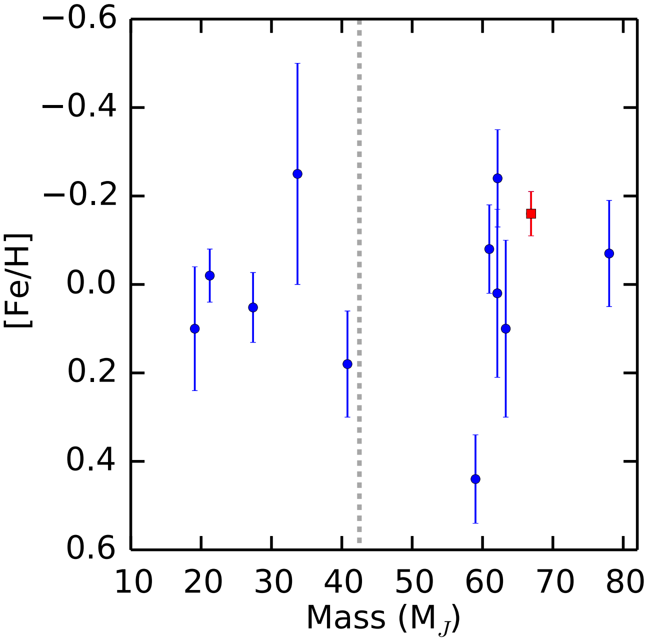

Figure 6. Stellar metallicities for all known main sequence stars that host transiting brown dwarfs. Data from the literature and this work (see Table 6). The red point indicates EPIC 201702477b and the gray dashed line indicates the 42.5 $M_{\rm J}$ limit. We do not see a corelation between the brown dwarf mass and and the host star metallicity, although this could be due to the small sample size of just 12 systems.

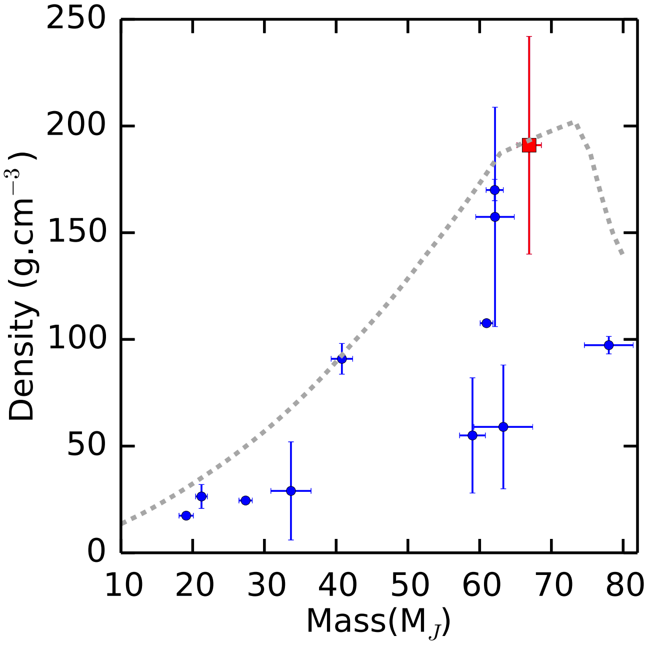

Figure 7. Density–mass relationship for the known transiting brown dwarfs. Sample and point symbols as for Figure 5. The gray dashed line indicates the COND03 model densities for brown dwarf of 8.8 Gyr—the estimated age of EPIC 201702477. We note that EPIC 201702477b stands out as the highest density object yet discovered, very near to the peak density predicted by the model. EPIC 201702477b has a density in perfect agreement with the 8.8 Gyr COND03 models.

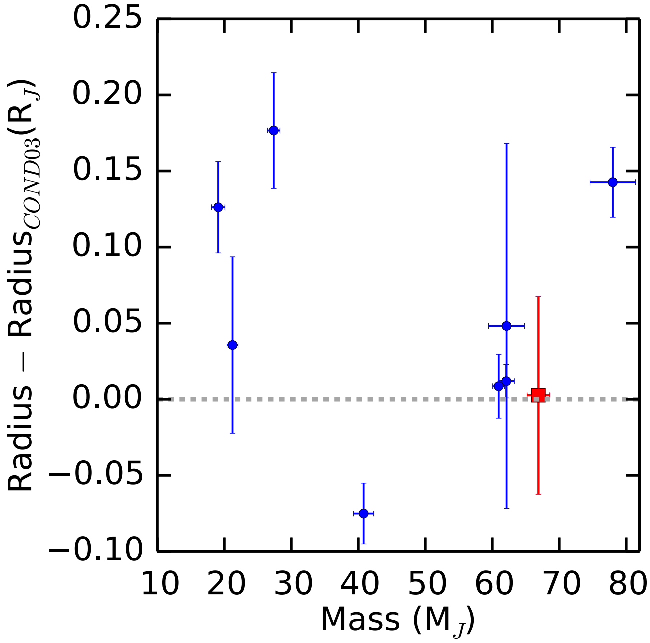

Figure 8. Residuals between the measured brown dwarf radius and the COND03 model radius (Baraffe et al. 2003) plotted against the brown dwarf mass. Sample and point symbols as for Figure 5, except that we only take systems which have well determined masses and radii (uncertainties <20%). The gray dashed-line indicates radii in perfect agreement with the COND03 models. We see the higher mass brown dwarfs, especially those between 60 and 70 $M_{\rm J}$, agree very well with the COND03 models, while lower mass systems appear to be inflated as compared to these models.

of 15–80 $M_{\rm J}$, the subsequent ejection process, which results in the loss of over half of the companions, is strongly mass dependent. Primarily it is the lower-mass brown dwarfs that are ejected, leaving behind a higher-mass population. These simulations even show that companions around 70 $M_{\rm J}$ are among the least likely to get ejected (see Figure 15 of Stamatellos & Whitworth 2009). It is possible that it is these objects we find as the population of transiting brown dwarfs with masses from 60 to 70 $M_{\rm J}$.

This work has been carried out within the framework of the National Centre for Competence in Research "PlanetS" supported by the Swiss National Science Foundation (SNSF). This paper includes data collected by the *K*2 mission. Funding for the *K*2 mission is provided by the NASA Science Mission directorate. This paper makes use of data and services from NASA Exoplanet Archive (Akeson et al. 2013), which is operated by the California Institute of Technology, under contract with the National Aeronautics and Space Administration under the Exoplanet Exploration Program. We are grateful to our colleagues who have performed some of the observations presented here with the HARPS spectrograph: F. Motalebi, A. Wyttenbach, and B. Lavie. The Porto group acknowledges the support from the Fundação para a Ciência e Tecnologia, FCT (Portugal) in the form of the grants, projects, and contracts UID/FIS/04434/2013 (POCI-01-0145-FEDER-007672), PTDC/FIS-AST/1526/2014 (POCI-01-0145-FEDER-016886), IF/00169/2012, IF/00028/2014, IF/01312/2014 and POPH/FSE (EC) by FEDER funding through the Programa Operacional de Factores de Competitividade—COMPETE.

Partly based on observations made at Observatoire de Haute Provence (CNRS), France and with ESO Telescopes at the La Silla Paranal Observatory under programme ID 096.C-0657. Some of the data presented herein were obtained at the W. M. Keck Observatory, which is operated as a scientific partnership among the California Institute of Technology, the

University of California and the National Aeronautics and Space Administration. The Observatory was made possible by the generous financial support of the W.M. Keck Foundation. The authors wish to recognize and acknowledge the very significant cultural role and reverence that the summit of Mauna Kea has always had within the indigenous Hawaiian community.

A.S. is supported by the European Union under a Marie Curie Intra-European Fellowship for Career Development with reference FP7-PEOPLE-2013-IEF, number 627202. J.L.-B. acknowledges financial support from the Marie Curie Actions of the European Commission (FP7-COFUND) and the Spanish grant AYA2012-38897-C02-01. J.M.A. acknowledges funding from the European Research Council under the ERC Grant Agreement n. 337591-ExTrA. D.J.A. and D.P. acknowledge funding from the European Union Seventh Framework programme (FP7/2007-2013) under grant agreement No. 313014 (ETAEARTH). O.D. acknowledges support by CNES through contract 567133. S.C.C.B. acknowledges support by the Fundação para a Ciência e Tecnologia, (FCT) through the Investigador FCT Contract No. IF/01312/2014 and the grant reference PTDC/FIS- AST/1526/2014.

K.H. and A.C.C. acknowledge support from UK Science and Technology Facilities Council (STFC) grant ST/M001296/1. D. Dragomir acknowledges support provided by NASA through Hubble Fellowship grant HST-HF2-51372.001-A awarded by the Space Telescope Science Institute, which is operated by the Association of Universities for Research in Astronomy, Inc., for NASA, under contract NAS5-26555. D.J. A.B. acknowledges support from the UKSA and the University of Warwick. B.J.F. notes that this material is based upon work supported by the National Science Foundation Graduate Research Fellowship under grant No. 2014184874. Any opinion, findings, and conclusions or recommendations expressed in this material are those of the authors(s) and do not necessarily reflect the views of the National Science Foundation. W.D.C. acknowledges support from NASA Grants NNX15AV58G and NNX16AE70G. This material is based upon work supported by the National Science Foundation Graduate Research Fellowship under Grant No. DGE-1144469 This work was performed in part under contract with the Jet Propulsion Laboratory (JPL) funded by NASA through the Sagan Fellowship Program executed by the NASA Exoplanet Science Institute.

Facilities: CAO:2.2m (AstraLux), ESO:3.6m (HARPS), *K2*, Keck:II (NIRC2), Keck:I (HIRES), LCOGT, OHP:1.93m (SOPHIE), ANU:2.3m (WiFeS).

REFERENCES

Akeson, R. L., Chen, X., Ciardi, D., et al. 2013, PASP, 125, 989
Anderson, D. R., Collier Cameron, A., Hellier, C., et al. 2011, ApJL, 726, L19
Bakos, G., Noyes, R. W., Kovács, G., et al. 2004, PASP, 116, 266
Baraffe, I., Chabrier, G., Barman, T. S., Allard, F., & Hauschildt, P. H. 2003, A&A, 402, 701
Baranne, A., Queloz, D., Mayor, M., et al. 1996, A&AS, 119, 373
Barros, S. C. C., Almenara, J. M., Demangeon, O., et al. 2015, MNRAS, 454, 4267
Barros, S. C. C., Demangeon, O., & Deleuil, M. 2016, A&A, 594, A100
Bayliss, D., Zhou, G., Penev, K., et al. 2013, AJ, 146, 113
Bessell, M. S. 1999, PASP, 111, 1426
Boisse, I., Eggenberger, A., Santos, N. C., et al. 2010, A&A, 523, A88
Bonomo, A. S., Sozzetti, A., Santerne, A., et al. 2015, A&A, 575, A85
Borucki, W. J., Koch, D., Basri, G., et al. 2010, Sci, 327, 977
Bouchy, F., Bonomo, A. S., Santerne, A., et al. 2011a, A&A, 533, A83
Bouchy, F., Deleuil, M., Guillot, T., et al. 2011b, A&A, 525, A68
Bouchy, F., Hébrard, G., Udry, S., et al. 2009a, A&A, 505, 853
Bouchy, F., Isambert, J., Lovis, C., et al. 2009b, in EAS Publications Ser. 37, ed. P. Kern (Les Ulis: EDP Sciences), 247
Bouchy, F., Pepe, F., & Queloz, D. 2001, A&A, 374, 733
Brahm, R., Jordán, A., Bakos, G. Á., et al. 2016, AJ, 151, 89
Brown, T. M., Baliber, N., Bianco, F. B., et al. 2013, PASP, 125, 1031
Chabrier, G., Johansen, A., Janson, M., & Rafikov, R. 2014, in Protostars and Planets VI, Giant Planet and Brown Dwarf Formation, ed. H. Beuther et al. (Tucson, AZ: Univ. Arizona Press), 619
Claret, A., & Bloemen, S. 2011, A&A, 529, A75
Csizmadia, S., Hatzes, A., Gandolfi, D., et al. 2015, A&A, 584, A13
Bakos, G. Á., Csubry, Z., Penev, K., et al. 2013, PASP, 125, 154
Deleuil, M., Deeg, H. J., Alonso, R., et al. 2008, A&A, 491, 889
Demory, B.-O., & Seager, S. 2011, ApJS, 197, 12
Díaz, R. F., Almenara, J. M., Santerne, A., et al. 2014a, MNRAS, 441, 983
Díaz, R. F., Damiani, C., Deleuil, M., et al. 2013, A&A, 551, L9
Díaz, R. F., Montagnier, G., Leconte, J., et al. 2014b, A&A, 572, A109
Dotter, A., Chaboyer, B., Jevremović, D., et al. 2008, ApJS, 178, 89
Eastman, J., Gaudi, B. S., & Agol, E. 2013, PASP, 125, 83
Fischer, D. A., & Valenti, J. 2005, ApJ, 622, 1102
Foreman-Mackey, D., Montet, B. T., Hogg, D. W., et al. 2015, ApJ, 806, 215
Gonzalez, G. 1997, MNRAS, 285, 403
Grether, D., & Lineweaver, C. H. 2006, ApJ, 640, 1051
Gustafsson, B., Edvardsson, B., Eriksson, K., et al. 2008, A&A, 486, 951
Halbwachs, J. L., Arenou, F., Mayor, M., Udry, S., & Queloz, D. 2000, A&A, 355, 581
Hormuth, F., Hippler, S., Brandner, W., Wagner, K., & Henning, T. 2008, Proc. SPIE, 7014, 701448
Howard, A. W., Johnson, J. A., Marcy, G. W., et al. 2010, ApJ, 721, 1467
Howell, S. B., Sobeck, C., Haas, M., et al. 2014, PASP, 126, 398
Irwin, J., Buchhave, L., Berta, Z. K., et al. 2010, ApJ, 718, 1353
Johnson, J. A., Apps, K., Gazak, J. Z., et al. 2011, ApJ, 730, 79
Kipping, D. M. 2013, MNRAS, 434, L51
Lillo-Box, J., Barrado, D., & Bouy, H. 2014, A&A, 566, A103
Lillo-Box, J., Ribas, A., Barrado, D., Merín, B., & Bouy, H. 2016, A&A, 592, A32
Ma, B., & Ge, J. 2014, MNRAS, 439, 2781
Marcy, G. W., & Butler, R. P. 2000, PASP, 112, 137
Mayor, M., Pepe, F., Queloz, D., et al. 2003, Msngr, 114, 20
Montet, B. T., Johnson, J. A., Muirhead, P. S., et al. 2015a, ApJ, 800, 134
Montet, B. T., Morton, T. D., Foreman-Mackey, D., et al. 2015b, ApJ, 809, 25
Mordasini, C., Alibert, Y., & Benz, W. 2009, A&A, 501, 1139
Morton, T. D. 2012, ApJ, 761, 6
Moutou, C., Bonomo, A. S., Bruno, G., et al. 2013, A&A, 558, L6
Nayakshin, S., & Fletcher, M. 2015, MNRAS, 452, 1654
Penev, K., Bakos, G. Á., Bayliss, D., et al. 2013, AJ, 145, 5
Pepper, J., Kuhn, R. B., Siverd, R., James, D., & Stassun, K. 2012, PASP, 124, 230
Petigura, E. A. 2015, PhD thesis, Univ. California
Pollacco, D. L., Skillen, I., Collier Cameron, A., et al. 2006, PASP, 118, 1407
Ricker, G. R., Winn, J. N., Vanderspek, R., et al. 2014, Proc. SPIE, 9143, 914320
Rouan, D., Baglin, A., Barge, P., et al. 1999, PCEC, 24, 567
Sahlmann, J., Ségransan, D., Queloz, D., et al. 2011, A&A, 525, A95
Santerne, A., Díaz, R. F., Almenara, J.-M., et al. 2015, MNRAS, 451, 2337
Santerne, A., Díaz, R. F., Moutou, C., et al. 2012, A&A, 545, A76
Santerne, A., Hébrard, G., Deleuil, M., et al. 2014, A&A, 571, A37
Santerne, A., Moutou, C., Tsantaki, M., et al. 2016, A&A, 587, A64
Santos, N. C., Israelian, G., & Mayor, M. 2001, A&A, 373, 1019
Siverd, R. J., Beatty, T. G., Pepper, J., et al. 2012, ApJ, 761, 123
Southworth, J. 2011, MNRAS, 417, 2166
Sozzetti, A., Torres, G., Charbonneau, D., et al. 2007, ApJ, 664, 1190
Stamatellos, D., & Whitworth, A. P. 2009, MNRAS, 392, 413
Stone, R. C. 1989, AJ, 97, 1227
Strehl, K. 1902, AN, 158, 89
Triaud, A. H. M. J., Queloz, D., Bouchy, F., et al. 2009, A&A, 506, 377
Troup, N. W., Nidever, D. L., De Lee, N., et al. 2016, AJ, 151, 85
Vanderburg, A., & Johnson, J. A. 2014, PASP, 126, 948
Vogt, S. S., Allen, S. L., Bigelow, B. C., et al. 1994, Proc. SPIE, 2198, 362
Wilson, P. A., Hébrard, G., Santos, N. C., et al. 2016, A&A, 588, A144